Title: Live Imaging Reveals the Cellular Events Downstream of SARM1 Activation

Kwang Woo Ko[1], Jeffrey Milbrandt[2, 3*], and Aaron DiAntonio[1, 3, 4 *]

[1]Department of Developmental Biology, Washington University School of Medicine, St. Louis, Missouri 63110, USA.
[2]Department of Genetics, Washington University School of Medicine, St. Louis, Missouri 63110, USA.
[3]Needleman Center for Neurometabolism and Axonal Therapeutics, Washington University School of Medicine, St. Louis, Missouri 63110, USA.
[4]Lead contact
* Corresponding authors: diantonio@wustl.edu, jmilbrandt@wustl.edu

Abstract

SARM1 is an inducible NAD^+ hydrolase that triggers axon loss and neuronal cell death in the injured and diseased nervous system. While SARM1 activation and enzyme function are well defined, the cellular events downstream of SARM1 activity but prior to axonal demise are much less well understood. Defects in calcium, mitochondria, ATP, and membrane homeostasis occur in injured axons, but the relationships among these events have been difficult to disentangle because prior studies analyzed large collections of axons in which cellular events occur asynchronously. Here we used live imaging with single axon resolution to investigate the cellular events downstream of SARM1 activity. Our studies support a model in which SARM1 NADase activity leads to an ordered sequence of events from loss of cellular ATP, to defects in mitochondrial movement and depolarization, followed by calcium influx, externalization of phosphatidylserine, and loss of membrane permeability prior to catastrophic axonal self-destruction.

Introduction

SARM1 is the central executioner of pathological axon degeneration, an early feature of many neurodegenerative diseases (Figley and DiAntonio, 2020; Krauss et al., 2020). SARM1 is the founding member of the TIR-domain family of NAD^+ hydrolases (Essuman et al., 2018, 2017), and a metabolic sensor activated by disrupted NAD^+ homeostasis (Figley et al., 2021; Gilley et al., 2015; Sasaki et al., 2016). Activation of the SARM1 NADase depletes cellular NAD^+ and initiates a metabolic crisis that ultimately leads to axon degeneration and/or neuronal cell death (Essuman et al., 2017; Gerdts et al., 2015). SARM1 is a compelling target for therapeutic intervention, as loss of SARM1 is profoundly protective in animal models of multiple neurodegenerative diseases including nerve injury, peripheral neuropathies, traumatic brain injury, glaucoma, retinitis pigmentosa, and Leber congenital amaurosis (Geisler et al., 2016; Gerdts et al., 2013; Henninger et al., 2016; Ko et al., 2020; Osterloh et al., 2012; Ozaki et al., 2020; Sasaki et al., 2020b; Turkiew et al., 2017). Moreover, as an enzyme, SARM1 is a druggable target, and both small molecule inhibitors and gene therapeutics effectively block axon degeneration (Bosanac et al., 2021; Geisler et al., 2019; Hughes et al., 2021). Recently, there has been tremendous progress in dissecting the structure of SARM1 (Bratkowski et al., 2020; Jiang et al., 2020; Sporny et al., 2020), the mechanism by which SARM1 is autoinhibited in healthy neurons (Shen et al., 2021) and activated in diseased neurons (Figley et al., 2021), and its role as an NAD^+ hydrolase (Essuman et al., 2017; Horsefield et al., 2019; Zhao et al., 2019). However, the events downstream of NAD^+ loss but prior to catastrophic axon fragmentation are much less well understood.

SARM1 and its NADase activity are essential for injury-induced axon degeneration, and the SARM1 enzyme is activated within 1-2 hours after injury in cultured DRG neurons (Sasaki et al., 2020a). Axonal fragmentation occurs much later in this system, with axons fragmenting approximately 4-6 hours after injury. Numerous molecular and cellular events occur in the time between SARM1 activation and axon loss, including calcium influx, mitochondrial stalling and depolarization, loss of ATP, and disrupted

membrane integrity. We reasoned that temporally ordering these events would give insights into causal relationships among these degenerative mechanisms. Unfortunately, studies in bulk culture are not appropriate for assessing the temporal sequence because axon loss is asynchronous, and so this effort requires live imaging. Prior live imaging studies have demonstrated that calcium influx precedes axonal fragmentation (Adalbert et al., 2012; Loreto et al., 2015; Vargas et al., 2015), however no comprehensive live imaging analysis of the cellular and molecular events underlying axon degeneration has been reported.

Here, we explore the cellular events that occur in injured axons following SARM1 activation. First, we investigate whether changes to mitochondria and calcium require SARM1 NADase activity, as prior studies used a complete knockout and so left open the possibility of NADase-independent functions. Indeed, such an NADase-independent function was recently described in *Drosophila* for organelle stalling after injury (Hsu et al., 2020). Next, we revisit the role of both intracellular and extracellular calcium in axon degeneration. We confirm that blocking extracellular calcium influx blocks axon fragmentation (Vargas et al., 2015; Villegas et al., 2014; Witte et al., 2019), however, these apparently morphologically intact axons are not metabolically active, as mitochondria are immobile and depolarized. We then develop a live imaging approach in cultured DRG neurons with single axon resolution and assess dynamic changes to calcium, mitochondria, ATP, and the plasma membrane. Our findings describe an ordered series of events in which 1) ATP is lost, 2) mitochondria stop moving and subsequently depolarize, 3) extracellular calcium enters the axons, 4) phosphatidylserine is exposed on the outer leaflet of the plasma membrane, and 5) the membrane losses integrity. This work identifies a stereotyped cascade of dysfunction following SARM1 activation, and highlights ATP loss as the likely key intermediate between NAD^+ cleavage and widespread dysfunction in injured axons.

Results

SARM1 NADase activity promotes mitochondrial stalling and calcium influx in injured axons

SARM1 is an injury-activated NAD^+ hydrolase, and this enzymatic activity is required for injury-induced axon degeneration (Essuman et al., 2017). However, it is unclear whether all SARM1-dependent processes require this enzymatic function. Recently, Hsu et al. working in *Drosophila* demonstrated that injury-dependent organelle stalling can be SARM1-dependent but NADase-independent (Hsu et al., 2020). Previously, Loreto et. al presented the even more surprising finding that injury-dependent mitochondrial stalling in superior cervical ganglion axons did not depend on SARM1, although loss of mitochondrial potential did depend on SARM1 (Loreto et al., 2015). Here we test the applicability of these findings to mammalian sensory neurons, assessing mitochondrial movement in cultured mouse dorsal root ganglion (DRG) neurons and assaying the requirement for SARM1 NADase activity. This is of particular interest because SARM1 is a mitochondrial associated protein and so alternate mechanisms of action are plausible. We cultured DRG neurons from SARM1 knockout (KO) embryos and used lentivirus to express either GFP, SARM1, or catalytically inactive SARM1(E642A) together with MitoDsRed (MitoDR) in order to track mitochondria. After seven days, axons were severed and mitochondrial movement was imaged 0, 2 and 4 hours after injury. In SARM1 KO neurons expressing GFP, mitochondrial movement was unchanged four hours after injury. In contrast, the number of motile mitochondria declines precipitously between 2 and 4 hours after injury in SARM1 KO axons re-expressing SARM1. Catalytically-inactive SARM1(E642A) is expressed at similar levels to wild-type (WT) SARM1 (Supplemental Fig. 1), but did not result in loss of mobile mitochondria after injury (Fig. 1A and 1B). Hence, the loss of mitochondrial mobility in injured axons is not only SARM1-dependent, but also SARM1 NADase-dependent. Injury-induced loss of mitochondrial potential is also SARM1-dependent (Loreto et al., 2015; Geisler et al., 2019), and so here we investigated whether or not this effect also requires a functional SARM1 NADase. The mitochondrial

potential is the driving force for ATP production and can be measured with the fluorescent dye TMRM (tetramethylrhodamine methy ester). As with mitochondrial dynamics, expression of WT SARM1, but not SARM1(E642A), leads to a dramatic loss of mitochondrial membrane potential after injury (Fig. 2C and 2D). The finding that SARM1 NADase activity is required for loss of mitochondrial membrane potential suggests that the SARM1-induced decline in cytosolic NAD^+ levels either directly or indirectly influences bioenergetics inside the mitochondria.

In addition to mitochondrial dysfunction, calcium homeostasis is also disrupted in injured axons (Adalbert et al., 2012; George et al., 1995; Ma et al., 2013; Yang et al., 2013). Here, we test if this calcium influx requires SARM1 enzymatic activity. We used Fluo-4, a calcium-sensitive fluorescent dye, to assess axonal calcium four hours after injury, the time point by which mitochondrial mobility and potential are disrupted. Axons show no calcium rise in SARM1 KO neurons expressing either GFP or SARM1(E642A), but have a significant increase in calcium when expressing WT SARM1 (Fig. 1E and 1F). Hence, the loss of calcium homeostasis in injured axons also requires SARM1 NADase activity. Taken together, these findings support the view that SARM1 enzyme activity is essential for not only axon degeneration (Essuman et al., 2017), but also for the major proximate events that occur in injured mammalian axons.

Manipulating either intracellular or extracellular calcium is ineffective in preserving injured axons

Having demonstrated that calcium influx into injured axons requires SARM1 NADase activity, we next explored the role of calcium influx in axonal demise. Prior studies argued that calcium release through the mitochondrial permeability transition pore (MPTP) (Barrientos et al., 2011; Villegas et al., 2014) or extracellular calcium influx (Vargas et al., 2015; Witte et al., 2019) are key drivers of axon degeneration. To test whether the MPTP has a role in axon degeneration, we incubated embryonic DRGs neurons with the MPTP inhibitor (Cyclosporin A, CsA), axotomized, and assessed the

progression of axon degeneration and the rise in intracellular calcium. In contrast to prior findings, we observed no delay in the timing of axon degeneration with CsA treatment (Fig. 2A). We also assayed the increase in intracellular calcium after injury and again found no significant effect of CsA (Fig. 2B). To further explore the role of intracellular calcium, we incubated DRG neurons with 10 µM BAPTA to chelate intracellular calcium for 30 minutes prior to axotomy. This treatment had no influence on the progression of axon degeneration (Fig. 2C). These results indicate that internal calcium is not a major determinant of injury-induced axon degeneration in this system, however it may play a role in scenarios where SARM1 is less potently activated (Li et al., 2021).

While we found no clear role for intracellular calcium, there are numerous studies highlighting the importance of extracellular calcium for injury-induced axon degeneration (Gerdts et al., 2011; Mishra et al., 2013; Ribas et al., 2017; Vargas et al., 2015; Yang et al., 2013). As such, we explored the impact of chelating extracellular calcium on the progression of axon degeneration. In agreement with prior studies, we find that pre-incubation with 3 mM EGTA maintained morphologically intact axons for up to 48 hours after axotomy (Fig. 2D and 2E). To explore when the influx of extracellular calcium is required, we treated with EGTA at the time of axotomy and then performed washout after 2 hours, or added the EGTA two hours after axotomy. The presence of EGTA from 0-2 hours after axotomy had no impact on the timing of axon fragmentation, while addition of EGTA two hours post-axotomy was as protective as treatment at the time of axotomy (Fig. 2D and 2E). Hence, late influx of extracellular calcium is critical for axon degeneration in DRG axons, a finding consistent with previous reports (Loreto et al., 2015; Vargas et al., 2015; Witte et al., 2019).

While these results are consistent with prior work highlighting the importance of extracellular calcium for axon degeneration, we did observe that severed axons developed prominent axonal swellings following extracellular calcium chelation (Fig. 2D, red arrowheads; (George et al., 1995)). Moreover, previous work showed that SARM1 is activated within two hours after injury and leads to NAD^+ depletion and metabolic

187 catastrophe (Sasaki et al., 2020a), raising the question of whether blocking the later
188 influx of calcium maintains axons in a healthy state. To investigate this question, we
189 assessed mitochondrial membrane potential and mobility in injured axons treated with
190 EGTA. We find that mitochondria potential is lost by four hours post-axotomy whether or
191 not EGTA is present (Fig. 2F and 2G). Similarly, EGTA treatment fails to maintain
192 mitochondrial mobility after axotomy (Fig. 2H and 2I). Indeed, treatment with EGTA
193 halts mitochondrial movement after four hours even in the absence of injury,
194 demonstrating that chelating extracellular calcium is not an effective method to maintain
195 healthy axons, and instead disrupts normal axonal physiology. These findings are in
196 contrast to loss of SARM1, which maintains both mitochondrial potential and mobility
197 after axotomy (Fig. 1). Taken together, these findings suggest that prior studies showing
198 protection of axons by blocking calcium influx were likely maintaining axonal structure
199 but not axonal physiology, and suggest that the key role for calcium influx may be to
200 trigger fragmentation of metabolically non-functional axons.
201
202
203 **Live single axon imaging defines the temporal relationship between calcium**
204 **influx and axonal fragmentation**
205
206 To quantitatively assess the relationship between calcium influx and axonal
207 fragmentation, we developed a live imaging system with single axon resolution
208 (Supplemental Fig. 2). This allows us to assess temporal relationships of the
209 asynchronous axon degeneration process that is not possible in mass cultures. We
210 used lentivirus to co-express GCaMP6 and mRuby3 in cultured DRG neurons to
211 monitor calcium influx and axon morphology simultaneously. After seven days in culture,
212 when both proteins were strongly expressed, we performed axotomy by focusing laser
213 light on a 1 x 1 µm region containing a single axon (Fig. 3A). Images of the distal axon
214 were repeatedly acquired until the injured axon degenerated. Figure 3B and
215 supplemental video 1 show the progression of calcium influx and axon degeneration for
216 a single axon, features that are representative of all the injured axons analyzed.
217 Immediately after axotomy, a first peak of calcium bidirectionally propagates along the

axon from the injury site (white triangle). This elevated intracellular calcium is rapidly cleared, demonstrating that calcium homeostasis functions normally at this time, and is consistent with the findings in Fig 2E that the initial influx of calcium does not contribute to axon fragmentation (Adalbert et al., 2012; Loreto et al., 2015; Vargas et al., 2015). After nearly four hours, there is a large second influx of calcium that precedes any obvious change in axonal morphology. Soon thereafter, the axon thins and small swellings appear, then the axon swellings enlarge, and finally the axon fragments (Fig. 3B and 3C). From analysis of 22 single axons, we found that the time to the appearance of the second calcium peak varied dramatically, from less than four hours to nearly ten hours after axotomy (Fig. 3D). However, once the second peak of calcium appeared, the axon fragmented soon thereafter. The correlation between the initiation of the 2nd peak of calcium and axon degeneration was very strong (Fig. 3D), with degeneration occurring ~100 minutes after initiation of calcium influx. In contrast, neither the duration nor intensity of the 2nd calcium peak was well correlated with the timing of axon degeneration (Fig. 3E and 3F). The very tight correlation between the initiation of the 2nd influx of calcium and axonal fragmentation is consistent with the hypothesis that this calcium triggers the final disintegration of the axon.

Mitochondrial dysfunction precedes calcium influx in injured axons.

With a method established for live imaging of single axons, we next explored the temporal relationship between calcium influx and mitochondrial stalling and loss of potential. Calcium influx is a potent mechanism for stopping mitochondria (Wang and Schwarz, 2009), and so we predicted that calcium influx would occur before mitochondrial stalling. We used lentivirus to express MitoDR and GCaMP6 in DRG neurons and performed laser axotomy. We imaged mitochondrial movement with MitoDR every 5 seconds for 300 seconds followed by calcium measurements. Images from MitoDR and GCaMP6 were acquired until mitochondria stopped, at which point only GCaMP6 imaging continued until its level increased more than 2-fold (Fig. 4A). As shown in Fig. 4A and in contrast to expectations, mitochondrial movement stops before

the influx of calcium. Analysis of this single axon shows that fewer mitochondria are moving three hours after axotomy (Fig 4B), and that all mitochondrial are stalled by 4.4 hours after injury (Fig. 4B, inset). At this point, the GCaMP6 signal is unchanged from baseline, but begins to rise soon thereafter. Quantitative analysis of single injured axons demonstrates that loss of mitochondrial mobility precedes calcium influx in each case, and this occurs ~25 minutes after mitochondria stop (Fig. 4B and 4C). Hence, loss of mitochondrial mobility in injured axons cannot be due to calcium influx.

Next, we addressed the relationship between loss of mitochondrial potential and calcium influx. Calcium overload can induce loss of mitochondrial potential (Abramov 2008)—if this occurs in injured axons, then we expect calcium influx to precede mitochondrial depolarization. We expressed GCaMP6 in DRG neurons, incubated the neurons with TMRM to assess mitochondrial potential, and imaged single axons in both channels every ten minutes until axons degenerated (Fig. 4D). This imaging frequency was chosen to avoid photobleaching. The images and analysis from a single axon (Fig. 4D and 4E) demonstrate that the fluorescent intensity of TMRM is fairly stable at baseline, then has an initial drastic drop (dark red dot in Fig. 4E) followed by a steady decline (Fig. 4E and 4F, red dots). In contrast, calcium has an abrupt rise (dark green dot), quickly reaching a higher steady-state level (Fig. 4E and 4F, green dots). In the example shown, the abrupt drop in mitochondrial potential occurs one frame prior to the large increase in calcium. To assess this across axons, we identified the time at which the TMRM and GCaMP6 signal showed the largest frame to frame variation (Fig. 4F and 4G and Supplemental Fig 3). We found that the drastic drop of TMRM intensity occurs one frame prior to the large increase in calcium in 5 out of 7 axons (71.43%), while these changes occurred during the same frame in 2 out of 7 axons. The images are taken ten minutes apart, and so these data indicate that in injured axons mitochondria begin depolarizing prior to the calcium influx (Fig. 4G). Moreover, these data, in conjunction with the analysis of mitochondrial mobility and calcium influx above, demonstrate a sequence of events in which first mitochondria stop, then begin losing their potential, and after that calcium enters the axon which subsequently degenerates.

ATP loss precedes mitochondrial stalling

Calcium influx cannot explain the loss of mitochondrial mobility, so we considered other potential mechanisms. Once the SARM1 NADase is activated, ATP is lost soon thereafter (Gerdts et al., 2015) because NAD^+ is required for ATP synthesis via both glycolysis and oxidative phosphorylation. In addition, mitochondria are transported by ATP-dependent molecular motors. Therefore, we hypothesized that loss of ATP may cause loss of mitochondrial mobility, and so explored the relationship between ATP loss and mitochondrial stalling. We used lentivirus to express PercevalHR, a sensor of relative ATP levels (Tantama et al., 2013), and MitoDR in DRG neurons and performed laser axotomy. We found that ATP loss and loss of mitochondrial mobility temporally overlap, and so it was not possible to define a window after which one process was complete and the other had yet to start, as we did with calcium and mitochondrial dynamics above. Instead, we quantitatively assessed the relationship between the degree of ATP loss as defined by loss of the PercevalHR signal and the fraction of mitochondria that stop moving in injured axons. Based on ATP measurements from bulk injured axons, we knew that most ATP loss occurred between 3 and 4 hours after injury (Sasaki et al., 2016). Therefore, we imaged baseline mitochondrial mobility and relative ATP levels before injury, and then re-imaged the PercevalHR every 5 minutes for 3.5 hours after single axon injury. We then calculated the percent change in PercevalHR intensity from baseline. Immediately after the final imaging of PercevalHR at 3.5 hours, we imaged mitochondrial mobility by acquiring images every 5 seconds for 300 seconds and calculated the percent drop in the fraction of motile mitochondria compared to baseline (Fig. 5A and 5B). In every axon the percent drop in the ATP sensor was larger than the percent drop in the fraction of mobile mitochondria (Fig. 5B left), and there was a strong correlation between the extent of ATP loss and mitochondrial stalling (Fig. 5B right; $R^2 = 0.61$, n=9). We continued to measure mitochondrial mobility from 3.5 hours after injury until mitochondrial movement ended. We found a strong inverse correlation between the extent of ATP loss at 3.5 hours and the remaining time until the complete loss of mitochondrial mobility (Fig. 5C; $R^2 = 0.76$, n=9). In other words, the extent of

ATP loss by 3.5 hours after injury is a strong predictor of when mitochondrial will ultimately stop moving in an injured axon. All of these results are consistent with the model that ATP loss causes loss of mitochondrial mobility.

Calcium is required for loss of membrane integrity during axon fragmentation

Having shown that calcium influx is a late event in the axon degeneration process, we assessed the temporal relationship between calcium influx and two other late events, loss of membrane lipid asymmetry and loss of membrane integrity. In healthy membranes, phosphatidylserine is preferentially found in the inner leaflet of the plasma membrane. In cells undergoing apoptosis and in degenerating axons, phosphatidylserine is exposed on the outer leaflet where it serves as an “eat-me” signal to phagocytic cells (Segawa and Nagata, 2015). To assess the temporal relationship among calcium influx, loss of membrane asymmetry, and axon fragmentation, we expressed GCaMP6 and mRuby3 in DRG neurons, laser axotomized, and incubated with Alex Fluor 647-conjugated Annexin-V, which binds extracellular phosphatidylserine (Sievers et al., 2003). In the example shown, calcium rises first, followed by staining with Annexin-V, and soon thereafter the mRuby3 signal declines indicative of axon fragmentation (Fig. 6A). Indeed, in all cells analyzed calcium influx preceded phosphatidylserine exposure, and occurred ~ 0.51 ± 0.04 (hr) prior to Annexin-V staining (Fig. 6B). Calcium can inhibit the ATP-dependent flippase that maintains phosphatidylserine on the inner leaflet (Bitbol et al., 1987; Soupene, 2008), and so the influx of calcium and/or the decline in ATP likely triggers the loss of membrane asymmetry during axon degeneration. We wished to test the role of calcium by blocking influx with EGTA, however this experiment is not possible because Annexin-V binding to phosphatidylserine requires extracellular calcium.

Next, we assessed the relationship among SARM1, calcium influx, and the loss of membrane integrity in injured axons. To assess membrane integrity, we applied

fluorescently labeled macromolecules (3kDa dextran) to neurons expressing cytosolic GFP. In uninjured neurons, cytosolic GFP fills the axon while the dextran is excluded (Fig. 6C). After injury, axon swelling is apparent, and mitochondrial localize to these swellings (Supplemental Fig. 4). The swellings retain GFP and still exclude dextran. Later, discrete puncta of dextran appear in axonal fragments, and such fragments contain no visible GFP. We interpret this as axon swellings that burst, releasing soluble GFP and allowing entry to the high molecular weight dextran (Fig. 6C). Next, we compared dextran uptake in injured axons from wild type and SARM1 KO neurons, as well as wild type neurons treated with EGTA. By four hours after axotomy of wild type neurons, dextran is present throughout the axons, indicative of a loss of membrane integrity. In axotomized SARM1 KO neurons, dextran is excluded from axons for at least 48 hours. Interestingly, when wild type neurons are incubated with EGTA, injured axons still swell (arrowheads, Fig. 6D), but dextran is excluded (Fig. 6D and 6E). Therefore, we conclude that calcium is necessary for the loss of membrane integrity and the morphological transition from axonal swelling to fragmentation.

Discussion

In injured axons, the molecular function of SARM1 is well understood, but the ensuing molecular and cellular changes leading to axonal demise are much more poorly defined. SARM1 NADase activity is critical for the ultimate demise of injured axons (Essuman et al., 2017), and here we show that this enzymatic activity is also required for intermediate phenotypes such as disrupted mitochondrial and calcium homeostasis. To explore the events that occur after NAD^+ cleavage, we used live imaging with single axon resolution to investigate dynamic changes to ATP, mitochondria, calcium, and membranes. The data describe an ordered series of events beginning with loss of ATP, and followed by mitochondrial dysfunction, calcium influx, exposure of phosphatidylserine and loss of membrane permeability ultimately resulting in catastrophic axon fragmentation.

In this study, we used live imaging of single axons to monitor structural and physiological changes during axon degeneration. While the absolute timing of cellular events varied dramatically from axon to axon, the relative timing was quite consistent. Hence, this method allowed us to order cellular events, which is not possible when averaging responses from many axons that are responding asynchronously. Our findings in conjunction with prior studies lead to a simple model of axon degeneration (Fig. 7). Following activation of SARM1, NAD^+ is cleaved and its levels drop rapidly. Upon robust NAD^+ depletion, both glycolysis and oxidative phosphorylation will be impaired, and so ATP production will decline. This loss of ATP will impact molecular motors, leading to the observed halting of mitochondria. Soon after mitochondria halt, they lose their membrane potential. Since this occurs before calcium increases, this cannot be due to calcium overload. Instead, the loss of NAD^+ and ATP likely disrupts mitochondrial homeostasis. We next observed influx of extracellular calcium. The loss of ATP is a likely culprit, as ionic pumps require ATP and their loss will lead to disrupted calcium extrusion, membrane depolarization, and calcium influx. The subsequent exposure of phosphatidylserine to the outer leaflet of the membrane is likely due to the failure of lipid flippases to maintain asymmetry. Since these flippases are ATP-dependent and can be inhibited by calcium (Bitbol et al., 1987; Pomorski and Menon, 2006; Soupene, 2008), loss of ATP and calcium influx may both contribute to the externalization of phosphatidylserine. The ultimate loss of membrane integrity, however, requires influx of extracellular calcium, as EGTA blocks fragmentation of injured axons. Such axons have extensive swellings and completely dysfunctional mitochondria. While calcium influx has long been assumed to the be the essential final step in axon loss, our findings suggest instead that calcium influx is merely leading to the morphological destruction of axons that are already physiologically dead. Instead, our findings highlight ATP loss as the likely point of no return for an injured axon, disrupting mitochondrial, calcium, and membrane homeostasis and thereby triggering axonal demise.

Methods

Animals

All procedures were performed in accordance with guidelines mandated in the National Institutes of Health Guide for the Care and Use of Laboratory Animals and approved by the Washington University School of Medicine in St. Louis Institutional Animal Care and Use committee. CD1 mice (gestation day 11.5) for sensory neuron cultures were purchased from Charles River Laboratories, and SARM1KO mice were a gift from M. Colonna at Washington University in St. Louis (Szretter et al., 2009).

Western blot analysis

Lysate buffers (60 mM Tri-HCl, pH 6.8; 50% glycerol; 2% SDS; 0.1% bromophenol blue) contain protease cocktail (cOmplete^{TM}, mini, EDTA-free protease inhibitor; 1183617001, Millipore Sigma) and phosphatase inhibitor cocktail (P0044, Millipore Sigma). The lysates were precleared of debris by centrifugation at 10,000 g in a refrigerated microcentrifuge for 10 mins. Supernatants were mixed with 5% 2-mercaptoethanol (Millipore Sigma) and then boiled for 10 mins. Antibodies used: Rabbit anti-β-Tubulin III (1:4,000, Millipore Sigma); HRP conjugated anti-rabbit antibody (1:10,000, #111-035-045, Jackson ImmunoResearch); Rabbit-anti-SARM1 (1:1,000, #13022, Cell signaling) and (1:5,000); mouse anti-GFP (1:1,000, #2955S, Cell signaling); HRP-conjugated anti-mouse antibody (1:5,000, 115-035-003, Jackson ImmunoResearch).

TMRM / Fluo-4

50 nM TMRM (T668, Thermo Fisher Scientific) and 1 µM Fluo-4 (F14201, Thermo Fisher Scientific) were pre-incubated for 30 minutes prior to image acquisition. When Fluo-4 was incubated more than 2 hours, we found that the intensity of Fluo-4 suddenly increased even in the absence of injury, and then axons degenerated. So, we only used Fluo-4 to check the current status of calcium and finished the imaging session within 1 hour.

Lentivirus construction/ production

FUGW-PercevalHR (Addgene #49083) GCaMP6 and mRuby3 (Ko et al., 2020), human SARM1.WT and human SARM1.E642A (Essuman et al., 2017) and MitoDsRed (Summers et al., 2014) were transfected into HEK 293 cells for lentivirus production. Briefly, the cells were seeded at 70~80% confluency per 35 mm well the day before transfection. The constructs (1.2 µg) were cotransfected with vesicular stomatitis virus G (600 ng) and pSPAX2 (800 ng) using FuGENE 6 (Promega). The lentiviral supernatants were collected 2 days after transfection, and then the cleared supernatant was concentrated with Lenti-X Concentrator (Clontech) to a final concentration of 1 ~ 10 x 10^7 particles / ml. Lentivirus transduction efficiency was monitored with tagged fluorophore and western blot analysis and is routinely ~100% in DRG neurons.

DRG neurons culture / Experimental timeline

All plates for DRG cultures are coated with 0.1 mg/ml poly-D-lysine (Millipore Sigma) followed by laminin (3 µg/ml; Invitrogen). CD1 mouse and SARM1 KO DRG neurons were dissected from embryonic day 13.5 or 14.5. They were incubated with 0.05% trypsin containing 0.05% EDTA at 37 ºC for 20 mins and then washed 3 times with DRG growth medium (neurobasal media from Gibco) containing 2% B27 (Invtrogen), 50 ng/ml nerve growth factor (Harlan Laboratories), 1 µM 5-fluoro-2'-deoxyuridine (Millipore Sigma), 1 µM uridine (Millipore Sigma), and penicillin/ streptomycin (Thermo Fisher Scientific). The cell density of these suspensions was adjusted to ~7 x 10^6 cells/ml. 2 µl suspensions were placed in 24-well plates (Corning) for western blots and axon degeneration assays, Chamber slides (Nunc™ Lab-Tek™, Thermo Fisher Scientific) were used for immunocytochemistry and FluoroDish (FD35-100, World Precision Instruments) were used for live single axon imaging. Lentivirus was transduced at 1 or 2 days in vitro (DIV). At DIV 7, assays for axon degeneration and/ or live axon imaging were performed.

DRG neuron culture for single axon imaging

For single axon imaging, conventional 2 µl suspensions (~7 x 10^6 DRG cells / ml) lead to extensive overlap of DRG axons making it difficult to distinguish individual axons. Moreover, DRG neurons did not survive well in low density culture (~7 x 10^4 cell / ml).

To circumvent these problems, we plated two different densities of DRG neurons in one Fluorodish (Supple. 3). Briefly, 2 µl suspensions (~7 x 10^6 cells/ml) were plated on one side of FluoroDish, and then 2 ul suspensions (~7 x 10^4 cells/ml) were thinly spread with a pipette tip on the other side of FluoroDish. This method provides the robust health of a high-density culture with the capacity to identify and image single axons.

Live single axon imaging

DRG neurons were cultured in a glass bottom FluoroDish, enabling use of an immersion oil objective for calcium (GCaMP6), mitochondrial movement (MitoDR) and potential (TMRM), ATP (PercevalHR), and axon morphology (GFP or mRuby3). At DIV 2, lentivirus was transduced to cultured DRG neurons. Chemical dyes such as Annexin-V (#A23204, Thermo Fisher Scientific) and 3 kDa Dextran-Texas Red (#D3328, Thermo Fisher Scientific) were applied according to product instructions. Chamlide TC™ (Live Cell Instrument, South Korea) was used to maintain 37 ºC temperature, 100 ml/min 5% CO_2/ 95% airflow rate. A Leica DMI4000B microscope under confocal setting using 20x oil immersion objective (NA 0.6) and Leica DFC7000 T 2.8 MP color microscope camera at RT was used under the control of the Leica Application Suite X software platform to acquire and analyze images. Optical sectioning and laser settings were kept constant across all image data acquisition sessions.

Laser Axotomy

Using a standard confocal microscope equipped with a 405-nm laser, a UV ablation method was utilized to selectively induce axonal injury of cultured DRG neurons in real-time (Fig. 3A). To effectively induce laser axotomy of culture DRG neurons, a glass bottom (<0.17 mm) culture dish such as FluoroDish is necessary. 405-nm laser with 100% intensity was used to induce laser axotomy with the FRAP (Fluorescence recovery after photobleaching) wizard in Leica application Suite X software. The injury site should be carefully chosen around the middle between the soma and axon terminal. If the injury site is close to soma, cell body death was often observed. If the injury site is too close to the distal axon, then the immediate retraction of the injured axon results in too little residual axon for imaging.

497

498 **Mitochondria movement / kymograph analysis**

499 For consecutive real-time imaging capture of mitochondria, images of MitoDR were
500 recorded at 5 seconds intervals for a total of 60 frames by 558 (ex) / 583 (em)-nm laser
501 at the designated time before and after laser axotomy. The mitochondria are considered
502 mobile if the net displacement is more than 5 μm. Otherwise, they are defined as
503 stationary.

504

505 **Data analysis**

506 *Axon degeneration*

507 Axon degeneration is quantified based on axon morphology as the axon degeneration
508 index (DI) using an ImageJ-based javascript (Sasaki et al., 2009). Axons should have
509 less than 0.2 DI at baseline, otherwise, they were not used for the experiment. We
510 define axon degeneration as an axon DI >0.4.

511

512 *Calcium influx*

513 The relative intensity of GCaMP6 from baseline was calculated as a measure of calcium
514 influx. Given the interval of 5 ~ 10 minutes between images, the intensity change of
515 GCaMP6 is dramatic. We defined a 2-fold increase or greater of GCaMP6 intensity from
516 the baseline as calcium influx.

517

518 *Axon continuity*

519 The intensity of mRuby3 was used to monitor the intactness of axons. Because mRuby3
520 is a cytosolic protein, as the integrity and thickness of axonal membrane is narrowed
521 and lost, the intensity of mRuby3 decreases. So, we defined more than 50% intensity
522 reduction of mRuby3 signal as the beginning of axon degeneration. When axonal
523 fragmentation is observed, it is defined as a degenerated axon regardless of mRuby3
524 intensity.

525

526 *TMRM*

After single axon injury, the intensity of TMRM were measured every 10 minutes (Fig. 4). We found that there was a less 10% fluctuation of fluorescent intensity between image frames. We calculated the percentage change of fluorescent intensity from the previous image (Diff_TMRM in Supple. 2), and then defined a more than 30% reduction as a significant loss of mitochondrial membrane potential.

Figures

Fig. 1. SARM1 enzymatic activity regulates mitochondrial movement and calcium homeostasis in injured axons

A. Representative kymograph of injured SARM1 KO axons expressing either GFP, SARM1, or SARM1.E642A (E642A). For imaging mitochondria movement, MitoDsRed lentivirus was transduced in all experimental conditions. Live cell imaging was performed at different times (0, 2, or 4 hr) after axon injury. Scale bar = 20 μm

B. Quantification of mobile mitochondria for the neurons in (A). Data represent the mean ± SEM; n = 5 ~ 13 for each condition; one-way ANOVA with post hoc Tukey test, $F(11,99) = 12.28$, $P<0.0001$; NS, not significant; *, $P<0.05$; **, $P<0.01$ and ***, $P<0.001$

C. Representative images of mitochondrial potential imaged with 50 nM TMRM fluorescent dye in SARM1 KO axons expressing either of GFP, SARM1, or SARM1.E642A. Live cell imaging was performed at the indicated times (0, 4, or 24 hr) after axon injury. Scale bar = 30 μm

D. Quantification of TMRM intensity from the experiment in (C). Injured SARM1 KO axons expressing the enzymatically disabled SARM1 mutant (E642A) maintained TMRM signal without significant loss. Data represent the mean ± SEM; n = 5 ~ 6 for each condition; one-way ANOVA with post hoc Tukey test, $F(4,23) = 53.11$, $P<0.0001$; NS, not significant; *, $P<0.05$; **, $P<0.01$ and ***, $P<0.001$

E. Representative images of calcium influx imaged with 1 μM Fluo-4 fluorescent dye in SARM1 KO axons expressing either of GFP, SARM1, or SARM1.E642A. Live cell imaging was performed at different times (0, or 4 hr) after axon injury. Scale bar = 30 μm

F. Quantification of Fluo-4 intensity from the experiment in (E). Injured SARM1 KO axons expressing the enzymatically disabled SARM1 mutant (E642A) completely prevent calcium influx. Data represent the mean ± SEM; n = 5 ~ 8 for each condition; one-way ANOVA with post hoc Tukey test, $F(3,22) = 23.05$, $P<0.0001$; NS, not significant; *, $P<0.05$; **, $P<0.01$ and ***, $P<0.001$

Fig. 2. The role of calcium in axon degeneration.

A. Pre-incubation of MPTP inhibitor (1, 10, or 100 µM CsA) did not significantly prevent the degeneration of wild-type axons after axon injury. Axon degeneration is defined as a degeneration index > 0.4 (dashed line). n = 3

B. (Left) Representative images of calcium influx acquired with 1 µM Fluo-4 dye. Scale bar = 30 µm (Right) The degree of calcium influx in CsA pre-incubated injured axons is not significantly different from DMSO pre-incubated injured axons. Fold increment of injured axons at 4 hr after axotomy is calculated from uninjured axons. Data represent the mean ± SEM; n = 5 for each condition; two-tailed unpaired t test, $p=0.39$; NS, not significant; *, $P<0.05$; **, $P<0.01$ and ***, $P<0.001$

C. Internal calcium chelator (pre-incubation with 10 µM BAPTA) did not delay axon degeneration after axonal injury.

D. (Top) Experimental design. Extracellular calcium chelator, 3 mM ETGA, was included in the culture medium at different time points (2 ~ 48 hr vs 0 ~ 2 hr vs 0 ~ 48 hr). For addition of EGTA from 0 ~ 2 hr, culture medium was replaced at 2 hr. (Bottom, left) Representative bright-field images of axons.

E. Quantification of axon degeneration for the experiment in (D). Although there are axonal swellings (red triangle) in the presence of EGTA, injured axons remain intact when the EGTA is present 2 hours after axotomy. n = 3

F. Representative images of mitochondria potential (TMRM fluorescent dye) and axon morphology (GFP lentivirus) in uncut axons and cut axons +/- EGTA. Scale bar = 100 μm

G. Quantification of the TMRM staining for the experiment in (F). EGTA incubation in injured axons does not maintain mitochondrial hyperpolarization. Data represent the mean ± SEM; n = 6 ~ 7 for each condition; one-way ANOVA with post hoc Tukey test, $F(2,16) = 98.27$, $P<0.0001$; NS, not significant; *, $P<0.05$; **, $P<0.01$ and ***, $P<0.001$

H. Representative kymograph of uncut and cut axons +/- EGTA as indicated.

I. Quantification of total number of mitochondria (left) and mobile mitochondria (right) for the experiment in (H). Data represent the mean ± SEM; n = 8 ~ 12 for each condition; one-way ANOVA with post hoc Tukey test, for mobile mitochondria $F(3,24) = 16.34$, $P<0.0001$; for number of mitochondria, $F(3,34) = 0.8787$, $P=0.46$; NS, not significant; *, $P<0.05$; **, $P<0.01$ and ***, $P<0.001$

Figure 3. Live single axon imaging enables temporal dissection of cellular events in injured axons.

A. Schematic diagram of laser axotomy in cultured embryonic DRG neurons. GCaMP6 and mRuby3 were expressed to observe calcium fluctuations and axonal morphology.

B. Snapshots of an injured wild-type axon. Also see supplemental video 1. Progression of axon degeneration is described at the bottom of the schematic. Note that there is both an early and late phase of calcium influx. The 1st peak of calcium occurs at the injury site (white triangle) before calcium levels return to normal. The 2nd calcium peak persists until the axon degenerates. Scale bar = 100 µm

C. Representative analysis of a single injured axon. The calcium response (left y-axis) and measure of axon continuity (right y-axis) for a single axon is plotted over time after axonal injury. Note the two distinct calcium peaks.

D-F. Grouped analysis from single axons for the (D) initiation, (E) duration, and (F) intensity of the 2nd peak of calcium compared to the time at which each axon fragments. The initiation of the second calcium peak occurs ~1.4 hrs before and is strongly correlated with axon fragmentation, while the duration of the second peak is weakly correlated and the intensity of the second peak is not correlated with axon fragmentation. n=22.

Figure 4. Mitochondrial dysfunction precedes calcium influx in injured axons.

A. (Top) Experimental design for observing calcium influx (GCaMP6) and mitochondria movement (MitoDR) after axon injury. MitoDR images were acquired every 5 seconds (for 300 second, 60 frames) followed by GCaMP6 imaging. Once the mitochondria in that axon stopped, GCaMP6 images were then acquired once/minute. (Bottom) Representative images of GCaMP6 and kymograph at the indicated times. Note that mitochondria stop prior to calcium influx. Scale bar = 30 µm

B. (Top) Single axon analysis after injury. The percentage of mobile mitochondria (red, left y-axis) and the fold change in calcium (green, right y-axis) for a single axon were

plotted over time after axonal injury. (Bottom) Inset from graph highlights that mitochondria stop moving before calcium levels rise.

C. Group data from single axons show that the time difference (ΔT) between cessation of mitochondrial mobility and calcium influx, defined as a 2-fold increase from baseline, is ~ 0.42 ± 0.02 hr, indicating that mitochondria stop before calcium influx in injured axons. The grey line ($\Delta T=0$) shows expected results if mitochondria stopped and calcium influx occurred simultaneously. n=9

D. (Top) Experimental design to observe calcium influx (GCaMP6) and loss of mitochondrial potential (TMRM) after axonal injury. GCaMP6 and TMRM were imaged every 10 minutes until axon fragmentation. (Bottom) Representative images shown at the indicated times. The TMRM signal declines by 2.83 hr after axonal injury, while calcium influx does not occur until 3.0 hr after injury. Scale bar = 30 μm

E. (Left) Analysis of the single axon in D. The ratio of TMRM signal from baseline (left y-axis) and the fold increment of calcium (right y-axis) were plotted over time after axonal injury. (Right) The enlarged insight highlights the point at which there is a dramatic change in the mitochondria potential (brighter red dot) and calcium levels (brighter green dot. Note that the change in TMRM from baseline precedes the change in calcium. This was observed in 5 out of 7 axons, while in 2 out of 7 axons the change occurred in the same 10 minute imaging bout.

Figure 5. ATP levels drop before mitochondria stop in injured axons.

A. (Left) Experimental design for imaging changes to ATP (PercevalHR) and mitochondrial movement (MitoDR) after axonal injury. Prior to axotomy, baseline PercevalHR intensity and mitochondrial movement were measured. PercevalHR was imaged every 5 minutes until 3.5 hr after axonal injury, while mitochondria were imaged every 5 minutes starting 3.5 hr after axotomy until movement ceased. (Right)

Representative images for PercevallHR and kymographs of moving mitochondria at the indicated times. Scale bar = 30 µm

B. (Left) Percentage decline from baseline at 3.5 hr post-axotomy for PercevalHR intensity and for the fraction of motile mitochondria. Lines connect data for individual cells. (Right) Linear regression plot of group data. n=9

C. The percentage decline of PercevalHR intensity at 3.5 hr after axonal injury is plotted against the subsequent time until mitochondria stop moving for that axon. Linear regression plot of group data. n=9

Figure 6. Calcium influx disrupts membrane integrity

A. (Left) Snapshots of representative live axon images for GCaMP6, mRuby3, and Alex647-conjugated Annexin-V at baseline, and 4.78 and 6.28 hr after axotomy. (Right) Representative single axon analysis. Y-axis (left) is plotted by the fold increase of fluorescent intensity (F / F_{base}) of either GCaMP6 (green color dots) or Annexin-V (cyan color dots) from the baseline after axon injury. Axon integrity (y-axis, right) is calculated by the relative mRuby3 intensity from the baseline. Note that calcium influx precedes Annexin-V exposure in an injured axon. Scale bar = 50 µm

B. After axotomy, the time until calcium influx is plotted vs the time until the rise in Annexin-V. Dashed line ($\Delta T=0$) represents the values if phosphatidylserine exposure (Annexin-V staining) and calcium influx occurred simultaneously. Calcium influx precedes phosphatidylserine exposure by an average of 0.51 ± 0.04 hr. n=10.

C. (Top) Representative images of intact, swollen, and fragmented axons during the process of axon degeneration. The axonal morphology is labelled with GFP that was transduced through GFP-lentivirus. Texas Red conjugated Dextran-3kDa was pre-

738 incubated 30 minutes prior to image acquisition. Note that Dextran-3kDa is only
739 observed in the fragmented axons, not in swollen axons. Scale bar = 10 µm
740
741 D. Representative images of GFP-expressing axotomized wild-type and SARM1 KO
742 axons. The membrane impermeable Dextran-3k enters injured wild-type axons, but after
743 injury is excluded from both EGTA-treated wild-type axons and SARM1 KO axons (GFP
744 labels axons). Scale bar = 100 µm
745
746 E. Group data. Quantification of dextran-3k staining intensity in the indicated genotypes
747 and times. Data represent the mean ± SEM; n = 6 for each condition; one-way ANOVA
748 with post hoc Tukey test, $F(6,35) = 46.16$, $P<0.0001$; NS, not significant; *, $P<0.05$; **,
749 $P<0.01$ and ***, $P<0.001$
750
751
752 **Figure 7. Model of Axon degeneration**
753 The model depicts the ordered series of events that occur in an injured axon following
754 SARM1 activation. These begin with NAD^+ loss, followed by ATP decline, loss of
755 mitochondrial mobility, loss of mitochondrial polarization, influx of calcium,
756 externalization of phosphatidylserine to the outer leaflet of the plasma membrane, and
757 finally fragmentation of the axon allowing for influx of large molecular weight dextrans.
758 Mitochondria localize to axonal swellings (see supplemental figure 4).
759
760 **Supplemental Figure 1. Expression level of SARM1.WT and SARM1.E642A**
761
762 Western blot analysis demonstrates that the lentiviral mediated expression of
763 SARM1.WT and SARM1.E642A is very similar.
764
765 **Supplemental Figure 2. Assessing mitochondrial potential and calcium influx in**
766 **injured axons**
767

(Left) Differentiation of TMRM and GCaMP6 measurements in Fig. 4E. The differentiation is defined as the percentage change from the previous intensity. The percentage change (y-axis) of both mitochondrial potential and calcium influx over the time after axon injury. (Right) This graph highlights the time window when calcium level (brighter green dot) increases at least 2-fold and mitochondria potential (brighter red dot) are maximally changed.

Supplemental Figure 3. DRG neuron culture for single axon imaging

For single axon imaging, 2 µl high-density cell suspensions (~7 x 10^6 cells / ml) were plated on the one side of a FluoroDish and 2 µl low-density cell suspensions (~7 x 10^4 cells / ml) were thinly spread on the opposite side. The high-density culture was required for maintenance of neurons in the low-density culture, and the low-density culture enabled imaging of single axons.

Supplemental Figure 4. Mitochondria accumulate in axonal swellings in injured axons

(Top) Representative images of injured (a) and uninjured (b) axons labelled with GFP and MitoDR. (Bottom) Pixel intensity of each axon is plotted. Note that most axonal swellings overlap with mitochondria (Asterisks).

Supplemental Video 1. Time lapse imaging of injured single axon

Total 45 second video. (0 ~ 20 seconds) Brief demonstration of experimental design for single axon imaging. (21 ~ 45 seconds) Example of Figure 3. Briefly, image the baseline activity at distal axon, followed by axon injury with a 405 nm laser (blue square). Note that there is an increase of GCaMP6 intensity at the injury site, which is the first peak of calcium. Massive calcium influx enters the injured distal axon and then later axon starts degenerate. Image acquisition of both GCaMP6 and mRuby3 continues until the axon degenerates.

Acknowledgements

We thank members of the DiAntonio and Milbrandt labs for fruitful discussions. This work was supported by National Institutes of Health grants R01CA219866 and RO1NS087632 (J.M. and A.D.) and RF1-AG013730 (J.M.).

Author contributions

K.W.K. and A.D. designed research. K.W.K performed all research and data analysis. K.W.K., J.M., and A.D. wrote the manuscript. J.M. and A.D. supervised experiments.

Competing of interests

A. DiAntonio and J. Milbrandt are cofounders, scientific advisory board members, and shareholders of Disarm Therapeutics, a wholly owned subsidiary of Eli Lilly and Company. The authors declare no additional competing financial interests.

References

Adalbert R, Morreale G, Paizs M, Conforti L, Walker SA, Roderick HL, Bootman MD, Siklós L, Coleman MP. 2012. Intra-axonal calcium changes after axotomy in wild-type and slow Wallerian degeneration axons. *Neuroscience* **225**:44–54. doi:10.1016/j.neuroscience.2012.08.056

Barrientos SA, Martinez NW, Yoo S, Jara JS, Zamorano S, Hetz C, Twiss JL, Alvarez J, Court FA. 2011. Axonal Degeneration Is Mediated by the Mitochondrial Permeability Transition Pore. *J Neurosci* **31**:966. doi:10.1523/JNEUROSCI.4065-10.2011

Bitbol M, Fellmann P, Zachowski A, Devaux PF. 1987. Ion regulation of phosphatidylserine and phosphatidylethanolamine outside-inside translocation in human erythrocytes. *BBA - Biomembr* **904**:268–282. doi:10.1016/0005-

2736(87)90376-2

Bosanac T, Hughes RO, Engber T, Devraj R, Brearley A, Danker K, Young K, Kopatz J, Hermann M, Berthemy A, Boyce S, Bentley J, Krauss R. 2021. Pharmacological SARM1 inhibition protects axon structure and function in paclitaxel-induced peripheral neuropathy. *Brain*. doi:10.1093/brain/awab184

Bratkowski M, Xie T, Thayer DA, Lad S, Mathur P, Yang YS, Danko G, Burdett TC, Danao J, Cantor A, Kozak JA, Brown SP, Bai X, Sambashivan S. 2020. Structural and Mechanistic Regulation of the Pro-degenerative NAD Hydrolase SARM1. *Cell Rep* **32**:107999. doi:10.1016/j.celrep.2020.107999

Essuman K, Summers DW, Sasaki Y, Mao X, DiAntonio A, Milbrandt J. 2017. The SARM1 Toll/Interleukin-1 Receptor Domain Possesses Intrinsic NAD+ Cleavage Activity that Promotes Pathological Axonal Degeneration. *Neuron* **93**:1334-1343.e5. doi:10.1016/j.neuron.2017.02.022

Essuman K, Summers DW, Sasaki Y, Mao X, Yim AKY, DiAntonio A, Milbrandt J. 2018. TIR Domain Proteins Are an Ancient Family of NAD+-Consuming Enzymes. *Curr Biol* **28**:421-430.e4. doi:10.1016/j.cub.2017.12.024

Figley MD, DiAntonio A. 2020. The SARM1 axon degeneration pathway: control of the NAD+ metabolome regulates axon survival in health and disease. *Curr Opin Neurobiol* **63**:59–66. doi:10.1016/j.conb.2020.02.012

Figley MD, Gu W, Nanson JD, Shi Y, Sasaki Y, Cunnea K, Malde AK, Jia X, Luo Z, Saikot FK, Mosaiab T, Masic V, Holt S, Hartley-Tassell L, McGuinness HY, Manik MK, Bosanac T, Landsberg MJ, Kerry PS, Mobli M, Hughes RO, Milbrandt J, Kobe B, DiAntonio A, Ve T. 2021. SARM1 is a metabolic sensor activated by an increased NMN/NAD+ ratio to trigger axon degeneration. *Neuron*. doi:10.1016/j.neuron.2021.02.009

Geisler S, Doan RA, Strickland A, Huang X, Milbrandt J, DiAntonio A. 2016. Prevention of vincristine-induced peripheral neuropathy by genetic deletion of SARM1 in mice. *Brain* **139**:3092–3108. doi:10.1093/brain/aww251

Geisler S, Huang SX, Strickland A, Doan RA, Summers DW, Mao X, Park J, DiAntonio A, Milbrandt J. 2019. Gene therapy targeting SARM1 blocks pathological axon degeneration in mice. *J Exp Med* **216**:294–303. doi:10.1084/jem.20181040

George EB, Glass JD, Griffin JW. 1995. Axotomy-induced axonal degeneration is mediated by calcium influx through ion-specific channels. *J Neurosci* **15**:6445–6452. doi:10.1523/jneurosci.15-10-06445.1995

Gerdts J, Brace EJ, Sasaki Y, DiAntonio A, Milbrandt J. 2015. SARM1 activation triggers axon degeneration locally via NAD+ destruction. *Science (80-)* **348**:453–457. doi:10.1126/science.1258366

Gerdts J, Sasaki Y, Vohra B, Marasa J, Milbrandt J. 2011. Image-based screening identifies novel roles for IκB kinase and glycogen synthase kinase 3 in axonal degeneration. *J Biol Chem* **286**:28011–28018. doi:10.1074/jbc.M111.250472

Gerdts J, Summers DW, Sasaki Y, DiAntonio A, Milbrandt J. 2013. Sarm1-Mediated Axon Degeneration Requires Both SAM and TIR Interactions. *J Neurosci* **33**:13569–13580. doi:10.1523/JNEUROSCI.1197-13.2013

Gilley J, Orsomando G, Nascimento-Ferreira I, Coleman MP. 2015. Absence of SARM1 Rescues Development and Survival of NMNAT2-Deficient Axons. *Cell Rep* **10**:1974–1981. doi:10.1016/j.celrep.2015.02.060

Henninger N, Bouley J, Sikoglu EM, An J, Moore CM, King JA, Bowser R, Freeman MR, Brown RH. 2016. Attenuated traumatic axonal injury and improved functional outcome after traumatic brain injury in mice lacking *Sarm1*. *Brain* **139**:1094–1105. doi:10.1093/brain/aww001

Horsefield S, Burdett H, Zhang X, Manik MK, Shi Y, Chen J, Qi T, Gilley J, Lai JS, Rank MX, Casey LW, Gu W, Ericsson DJ, Foley G, Hughes RO, Bosanac T, Von Itzstein M, Rathjen JP, Nanson JD, Boden M, Dry IB, Williams SJ, Staskawicz BJ, Coleman MP, Ve T, Dodds PN, Kobe B. 2019. NAD+ cleavage activity by animal and plant TIR domains in cell death pathways. *Science (80-)* **365**:793–799. doi:10.1126/science.aax1911

Hsu JM, Kang Y, Corty MM, Mathieson D, Peters OM, Freeman MR. 2020. Injury-Induced Inhibition of Bystander Neurons Requires dSarm and Signaling from Glia. *Neuron* **0**. doi:10.1016/j.neuron.2020.11.012

Hughes RO, Bosanac T, Mao X, Engber TM, DiAntonio A, Milbrandt J, Devraj R, Krauss R. 2021. Small Molecule SARM1 Inhibitors Recapitulate the SARM1−/− Phenotype and Allow Recovery of a Metastable Pool of Axons Fated to Degenerate. *Cell Rep*

34:108588. doi:10.1016/j.celrep.2020.108588

Jiang Y, Liu T, Lee CH, Chang Q, Yang J, Zhang Z. 2020. The NAD+-mediated self-inhibition mechanism of pro-neurodegenerative SARM1. *Nature* **588**:658–663. doi:10.1038/s41586-020-2862-z

Ko KW, Milbrandt J, DiAntonio A. 2020. SARM1 acts downstream of neuroinflammatory and necroptotic signaling to induce axon degeneration. *J Cell Biol* **219**. doi:10.1083/jcb.201912047

Krauss R, Bosanac T, Devraj R, Engber T, Hughes RO. 2020. Axons Matter: The Promise of Treating Neurodegenerative Disorders by Targeting SARM1-Mediated Axonal Degeneration. *Trends Pharmacol Sci*. doi:10.1016/j.tips.2020.01.006

Li Y, Pazyra-Murphy MF, Avizonis D, De Sa M, Russo T, Tang S, Bergholz JS, Jiang T, Zhao JJ, Zhu J, Ko KW, Milbrandt J, Diantonio A, Segal RA. 2021. Title: Activation of Sarm1 produces cADPR to increase intra-axonal calcium and promote axon degeneration in CIPN. *bioRxiv* 2021.04.15.440024. doi:10.1101/2021.04.15.440024

Loreto A, Di Stefano M, Gering M, Conforti L. 2015. Wallerian Degeneration Is Executed by an NMN-SARM1-Dependent Late Ca2+ Influx but Only Modestly Influenced by Mitochondria. *Cell Rep* **13**:2539–2552. doi:10.1016/J.CELREP.2015.11.032

Ma M, Ferguson TA, Schoch KM, Li J, Qian Y, Shofer FS, Saatman KE, Neumar RW. 2013. Calpains mediate axonal cytoskeleton disintegration during Wallerian degeneration. *Neurobiol Dis* **56**:34–46. doi:10.1016/j.nbd.2013.03.009

Mishra B, Carson R, Hume RI, Collins CA. 2013. Sodium and potassium currents influence wallerian degeneration of injured Drosophila axons. *J Neurosci* **33**:18728–18739. doi:10.1523/JNEUROSCI.1007-13.2013

Osterloh JM, Yang J, Rooney TM, Fox AN, Adalbert R, Powell EH, Sheehan AE, Avery MA, Hackett R, Logan MA, MacDonald JM, Ziegenfuss JS, Milde S, Hou Y-J, Nathan C, Ding A, Brown RH, Conforti L, Coleman M, Tessier-Lavigne M, Zuchner S, Freeman MR. 2012. dSarm/Sarm1 Is Required for Activation of an Injury-Induced Axon Death Pathway. *Science (80-)* **337**:481–484. doi:10.1126/science.1223899

Ozaki E, Gibbons L, Neto NGB, Kenna P, Carty M, Humphries M, Humphries P, Campbell M, Monaghan M, Bowie A, Doyle SL. 2020. SARM1 deficiency promotes

923 rod and cone photoreceptor cell survival in a model of retinal degeneration. *Life Sci*
924 *Alliance* **3**. doi:10.26508/lsa.201900618
925 Pomorski T, Menon AK. 2006. Lipid flippases and their biological functions. *Cell Mol Life*
926 *Sci*. doi:10.1007/s00018-006-6167-7
927 Ribas VT, Koch JC, Michel U, Bähr M, Lingor P. 2017. Attenuation of Axonal
928 Degeneration by Calcium Channel Inhibitors Improves Retinal Ganglion Cell
929 Survival and Regeneration After Optic Nerve Crush. *Mol Neurobiol* **54**:72–86.
930 doi:10.1007/s12035-015-9676-2
931 Sasaki Y, Engber TM, Hughes RO, Figley MD, Wu T, Bosanac T, Devraj R, Milbrandt J,
932 Krauss R, DiAntonio A. 2020a. cADPR is a gene dosage-sensitive biomarker of
933 SARM1 activity in healthy, compromised, and degenerating axons. *Exp Neurol*
934 **329**:113252. doi:10.1016/j.expneurol.2020.113252
935 Sasaki Y, Kakita H, Kubota S, Sene A, Lee TJ, Ban N, Dong Z, Lin JB, Boye SL, Di
936 Antonio A, Boye SE, Apte RS, Milbrandt J. 2020b. SARM1 depletion rescues
937 NMNAT1-dependent photoreceptor cell death and retinal degeneration. *Elife* **9**:1–
938 19. doi:10.7554/eLife.62027
939 Sasaki Y, Nakagawa T, Mao X, DiAntonio A, Milbrandt J. 2016. NMNAT1 inhibits axon
940 degeneration via blockade of SARM1-mediated NAD+depletion. *Elife* **5**:e19749.
941 doi:10.7554/eLife.19749
942 Sasaki Y, Vohra BPS, Lund FE, Milbrandt J. 2009. Nicotinamide mononucleotide
943 adenylyl transferase-mediated axonal protection requires enzymatic activity but not
944 increased levels of neuronal nicotinamide adenine dinucleotide. *J Neurosci*
945 **29**:5525–35. doi:10.1523/JNEUROSCI.5469-08.2009
946 Segawa K, Nagata S. 2015. An Apoptotic “Eat Me” Signal: Phosphatidylserine Exposure.
947 *Trends Cell Biol*. doi:10.1016/j.tcb.2015.08.003
948 Shen C, Vohra M, Zhang P, Mao X, Figley MD, Zhu J, Sasaki Y, Wu H, DiAntonio A,
949 Milbrandt J. 2021. Multiple domain interfaces mediate SARM1 autoinhibition. *Proc*
950 *Natl Acad Sci U S A* **118**:2021. doi:10.1073/pnas.2023151118
951 Sievers C, Platt N, Perry VH, Coleman MP, Conforti L. 2003. Neurites undergoing
952 Wallerian degeneration show an apoptotic-like process with annexin V positive
953 staining and loss of mitochondrial membrane potential. *Neurosci Res* **46**:161–169.

doi:10.1016/S0168-0102(03)00039-7

Soupene E. 2008. ATP8A1 activity and phosphatidylserine transbilayer movement. *J Receptor Ligand Channel Res* **Volume 1**:1–10. doi:10.2147/jrlcr.s3773

Sporny M, Guez-Haddad J, Khazma T, Yaron A, Dessau M, Shkolnisky Y, Mim C, Isupov MN, Zalk R, Hons M, Opatowsky Y. 2020. Structural basis for sarm1 inhibition and activation under energetic stress. *Elife* **9**:1–25. doi:10.7554/eLife.62021

Summers DW, DiAntonio A, Milbrandt J. 2014. Mitochondrial dysfunction induces Sarm1-dependent cell death in sensory neurons. *J Neurosci* **34**:9338–50. doi:10.1523/JNEUROSCI.0877-14.2014

Szretter KJ, Samuel MA, Gilfillan S, Fuchs A, Colonna M, Diamond MS. 2009. The Immune Adaptor Molecule SARM Modulates Tumor Necrosis Factor Alpha Production and Microglia Activation in the Brainstem and Restricts West Nile Virus Pathogenesis. *J Virol* **83**:9329–9338. doi:10.1128/jvi.00836-09

Tantama M, Martínez-François JR, Mongeon R, Yellen G. 2013. Imaging energy status in live cells with a fluorescent biosensor of the intracellular ATP-to-ADP ratio. *Nat Commun* **4**:2550. doi:10.1038/ncomms3550

Turkiew E, Falconer D, Reed N, Höke A. 2017. Deletion of Sarm1 gene is neuroprotective in two models of peripheral neuropathy. *J Peripher Nerv Syst* **22**:162–171. doi:10.1111/jns.12219

Vargas ME, Yamagishi Y, Tessier-Lavigne M, Sagasti A. 2015. Live imaging of calcium dynamics during axon degeneration reveals two functionally distinct phases of calcium influx. *J Neurosci* **35**:15026–15038. doi:10.1523/JNEUROSCI.2484-15.2015

Villegas R, Martinez NW, Lillo J, Pihan P, Hernandez D, Twiss JL, Court FA. 2014. Calcium release from intra-axonal endoplasmic reticulum leads to axon degeneration through mitochondrial dysfunction. *J Neurosci* **34**:7179–7189. doi:10.1523/JNEUROSCI.4784-13.2014

Wang X, Schwarz TL. 2009. The Mechanism of Ca2+-Dependent Regulation of Kinesin-Mediated Mitochondrial Motility. *Cell* **136**:163–174. doi:10.1016/j.cell.2008.11.046

Witte ME, Schumacher A-M, Mahler CF, Bewersdorf JP, Lehmitz J, Scheiter A,

985 Sánchez P, Williams PR, Griesbeck O, Naumann R, Misgeld T, Kerschensteiner M.
986 2019. Calcium Influx through Plasma-Membrane Nanoruptures Drives Axon
987 Degeneration in a Model of Multiple Sclerosis. *Neuron* **101**:615–624.
988 doi:10.1016/J.NEURON.2018.12.023
989 Yang J, Weimer RMM, Kallop D, Olsen O, Wu Z, Renier N, Uryu K, Tessier-Lavigne M.
990 2013. Regulation of Axon Degeneration after Injury and in Development by the
991 Endogenous Calpain Inhibitor Calpastatin. *Neuron* **80**:1175–1189.
992 doi:10.1016/J.NEURON.2013.08.034
993 Zhao ZY, Xie XJ, Li WH, Liu J, Chen Z, Zhang B, Li T, Li SL, Lu JG, Zhang Liangren,
994 Zhang Li he, Xu Z, Lee HC, Zhao YJ. 2019. A Cell-Permeant Mimetic of NMN
995 Activates SARM1 to Produce Cyclic ADP-Ribose and Induce Non-apoptotic Cell
996 Death. *iScience* **15**:452–466. doi:10.1016/j.isci.2019.05.001
997

Fig. 1

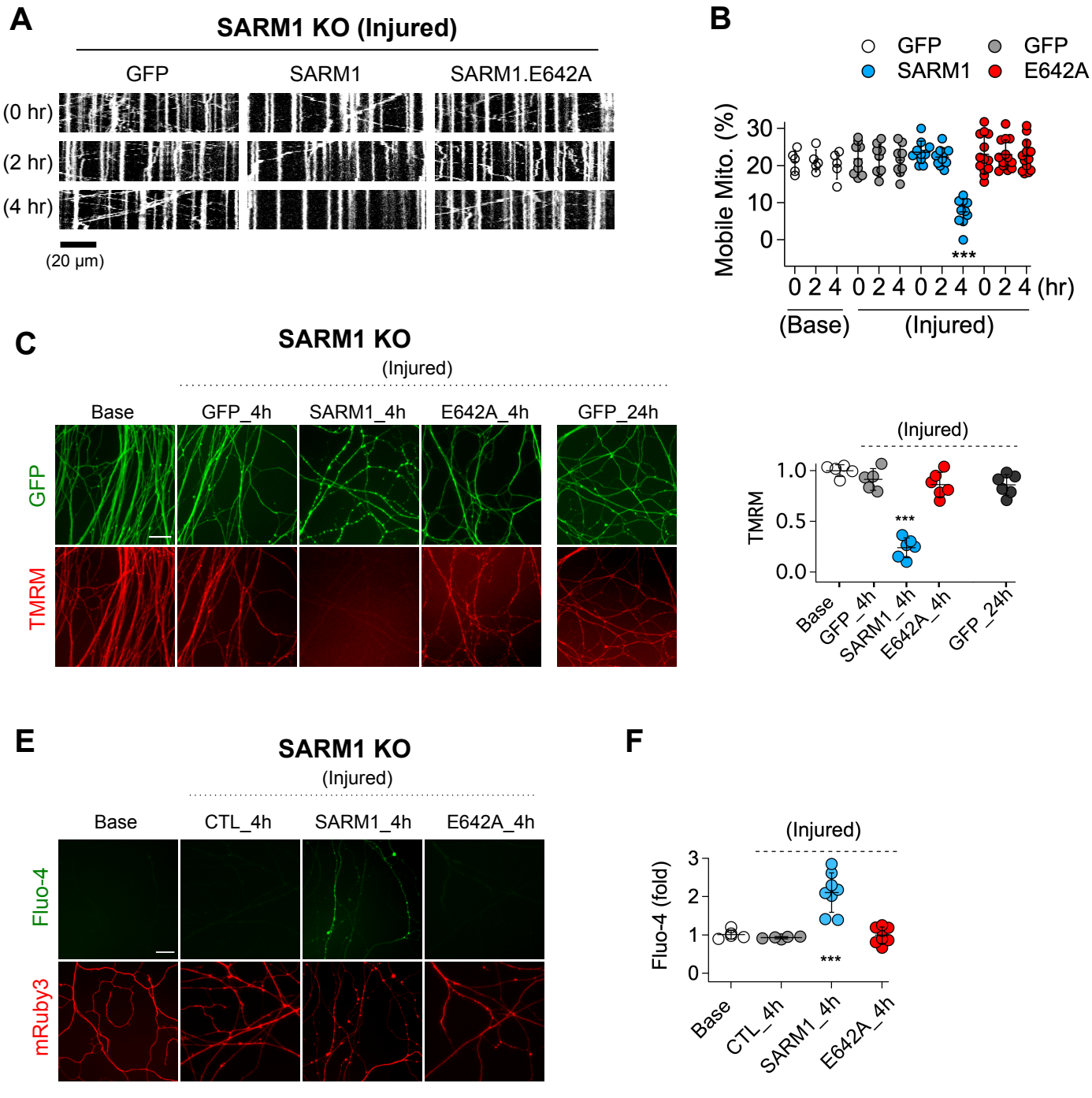

Fig. 2

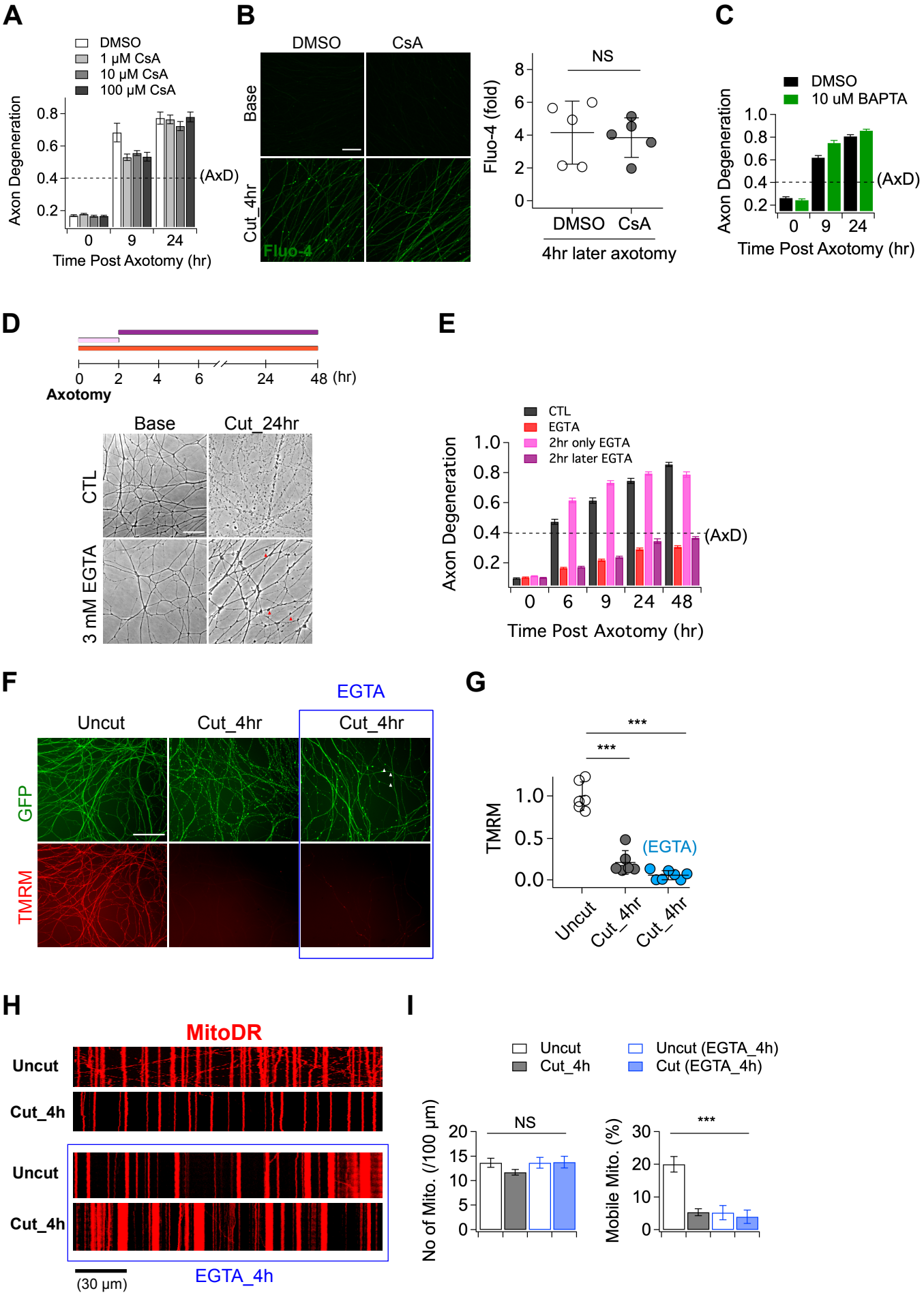

Fig. 3

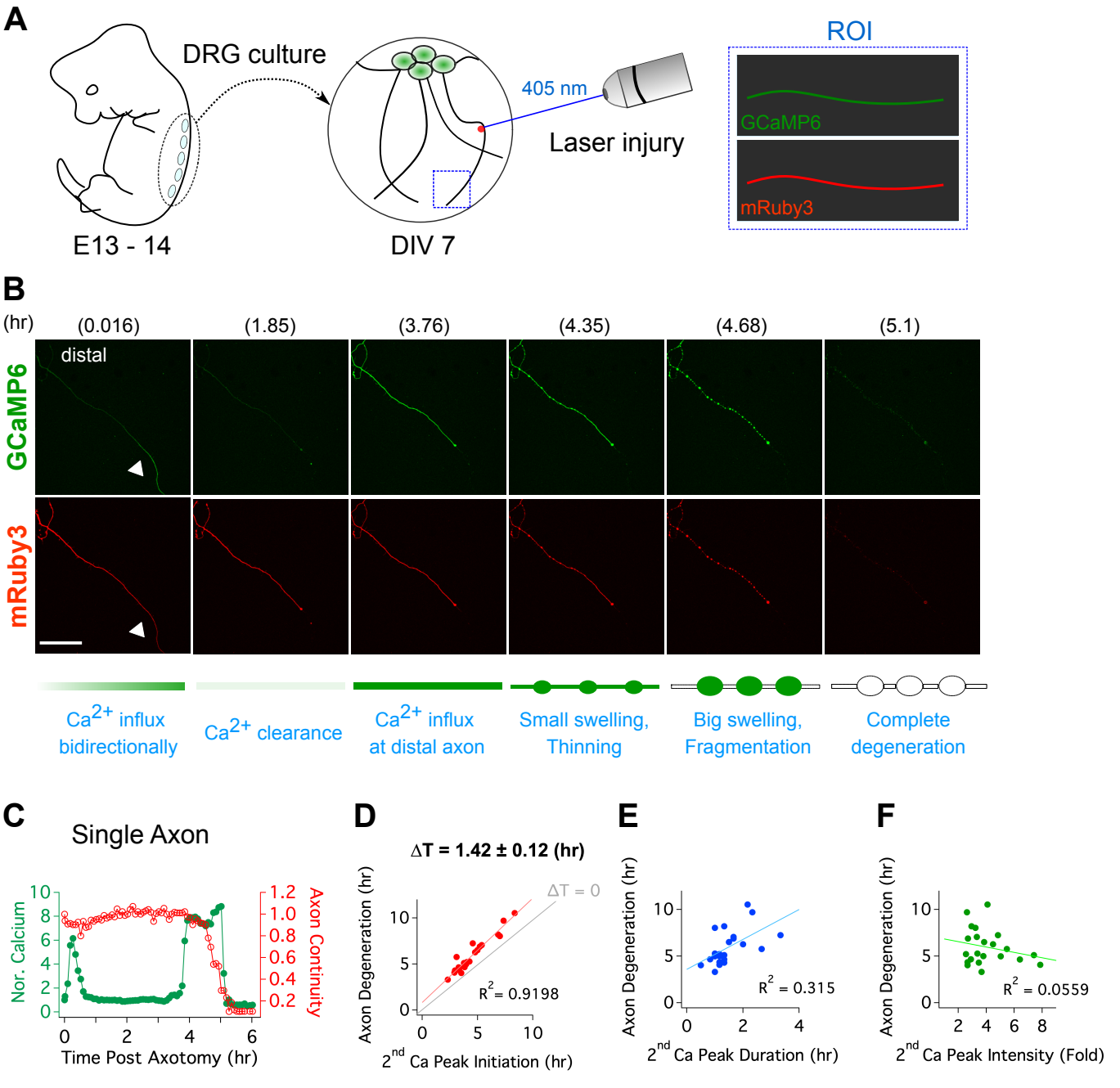

Fig. 4

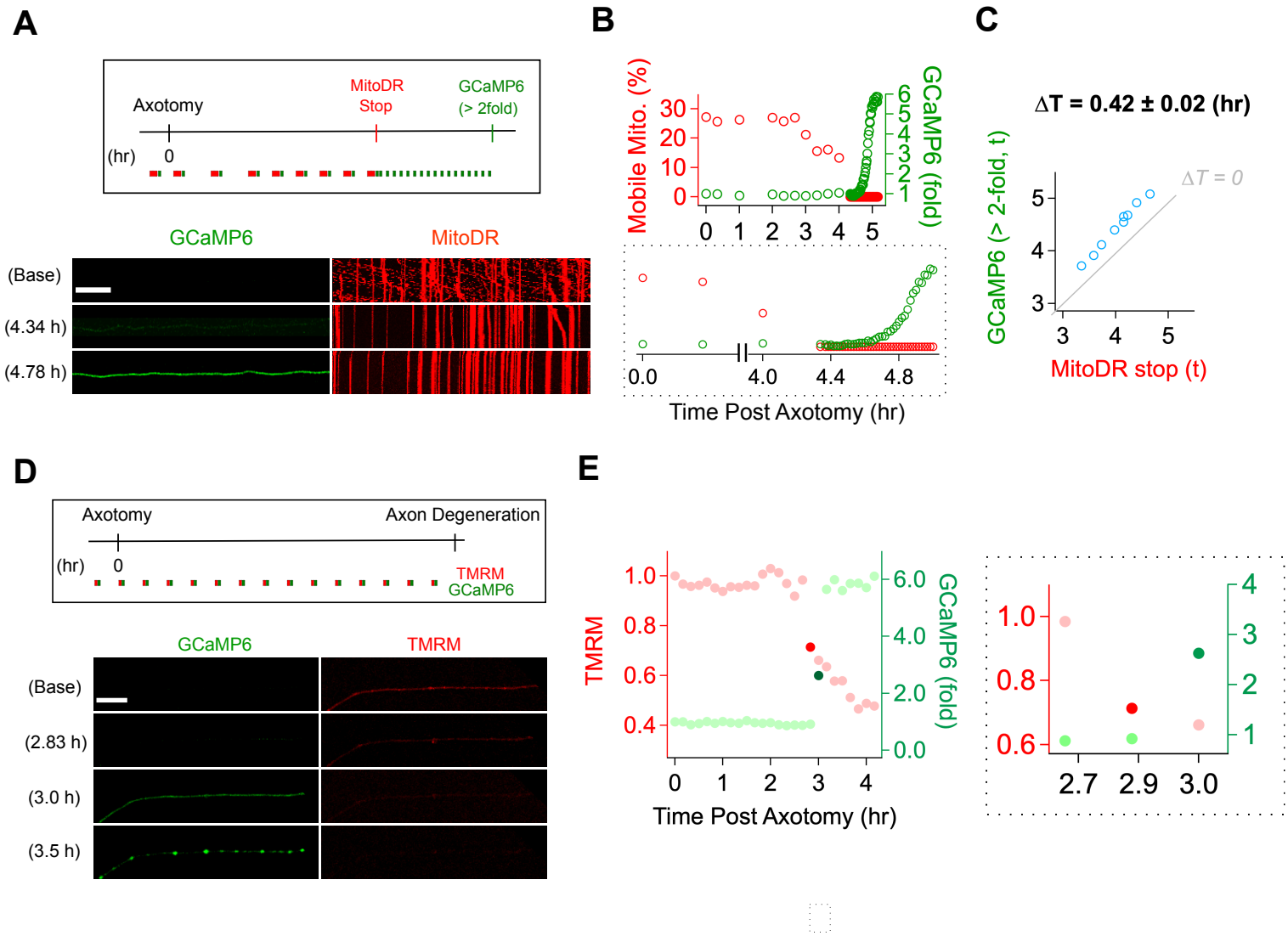

Fig. 5

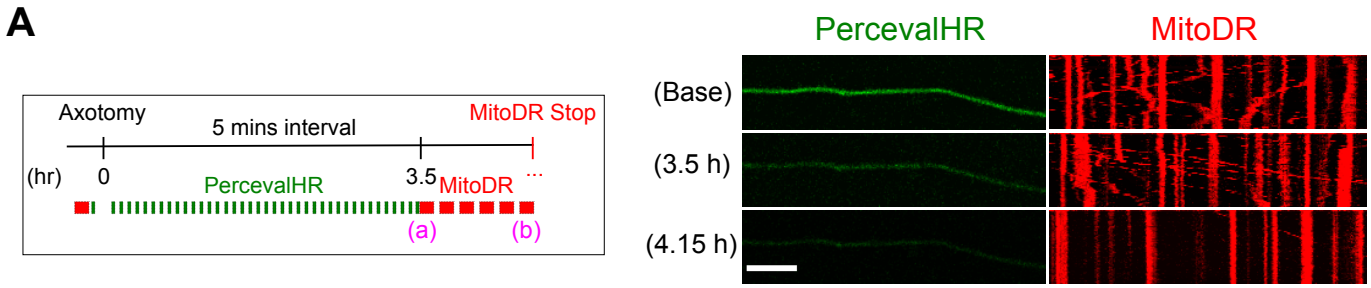

Fig. 6

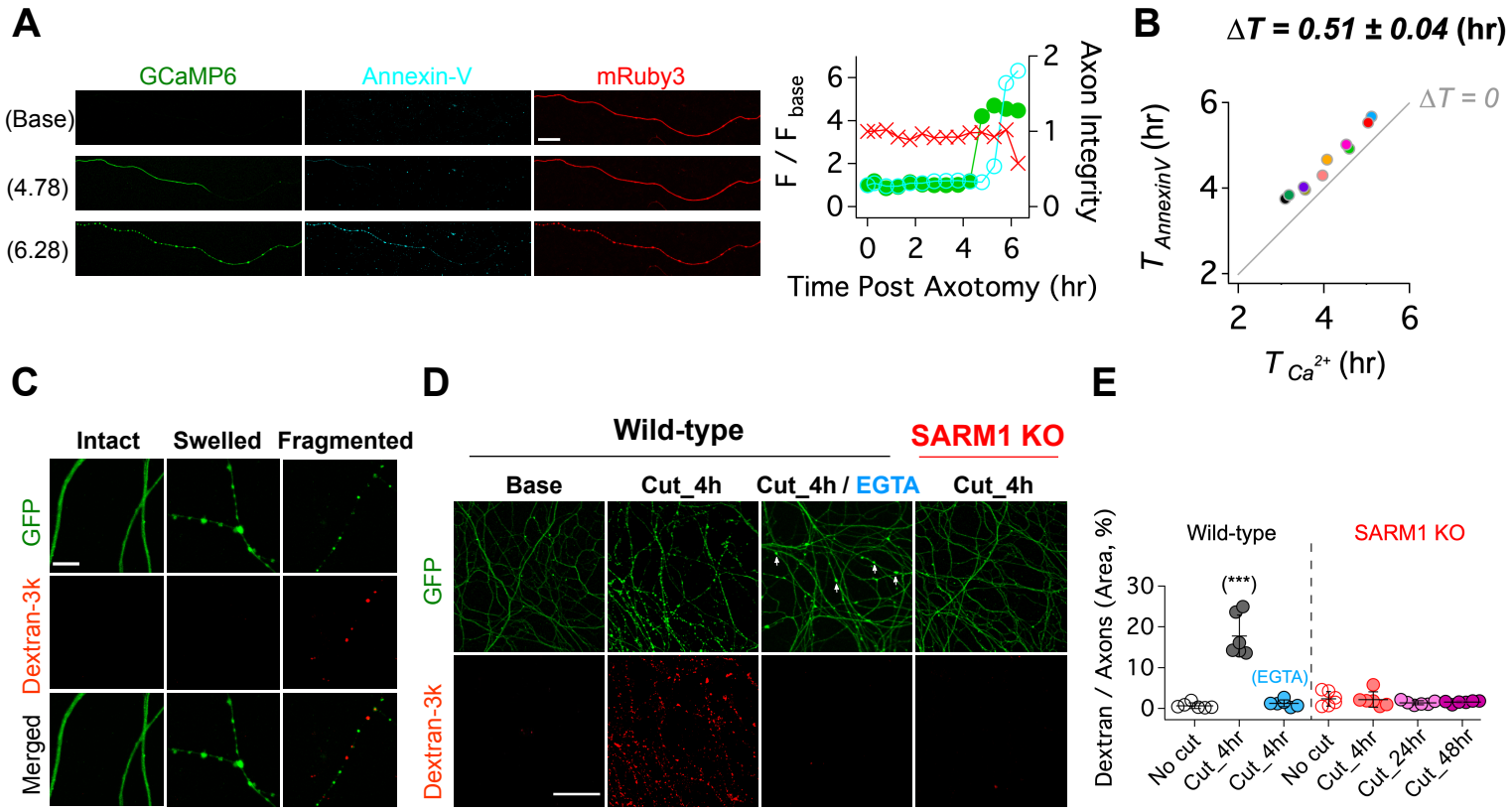

Fig. 7

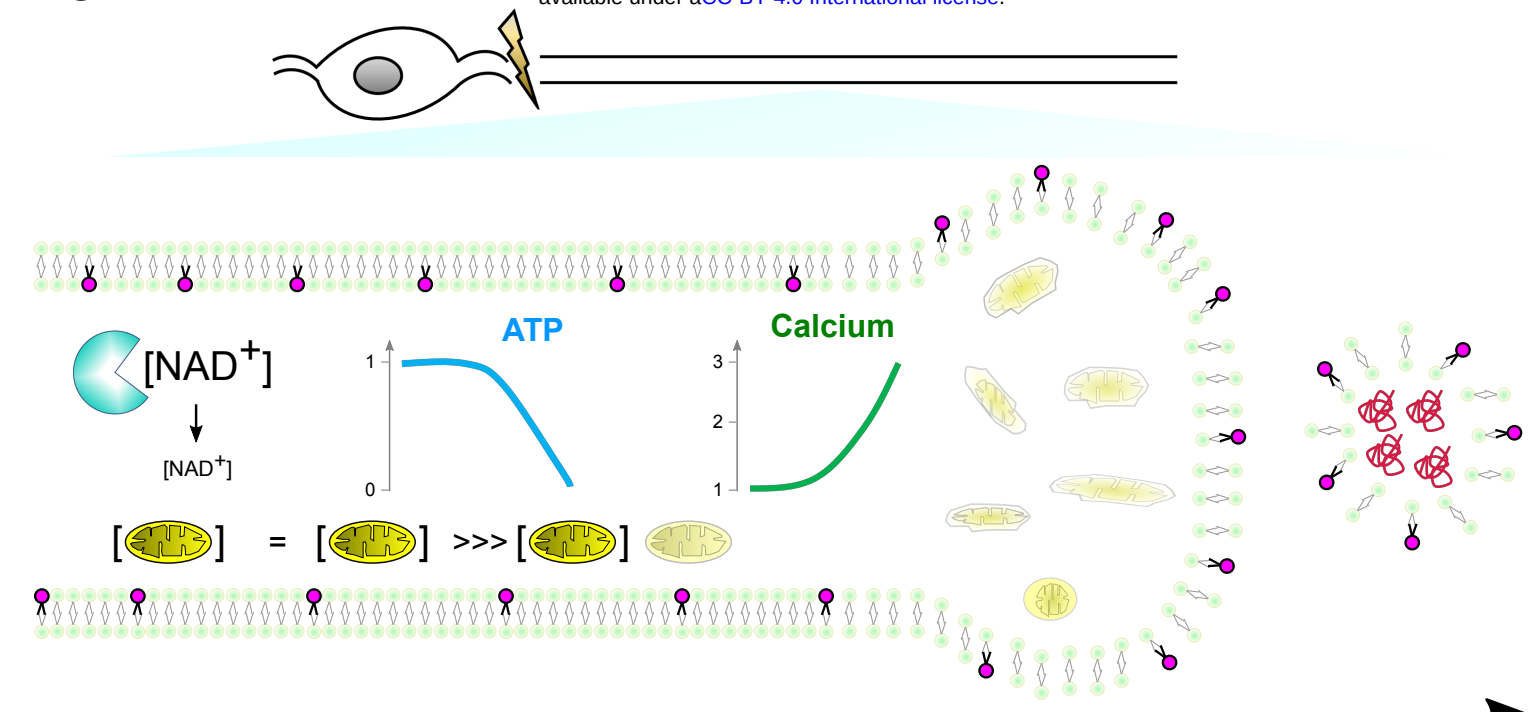

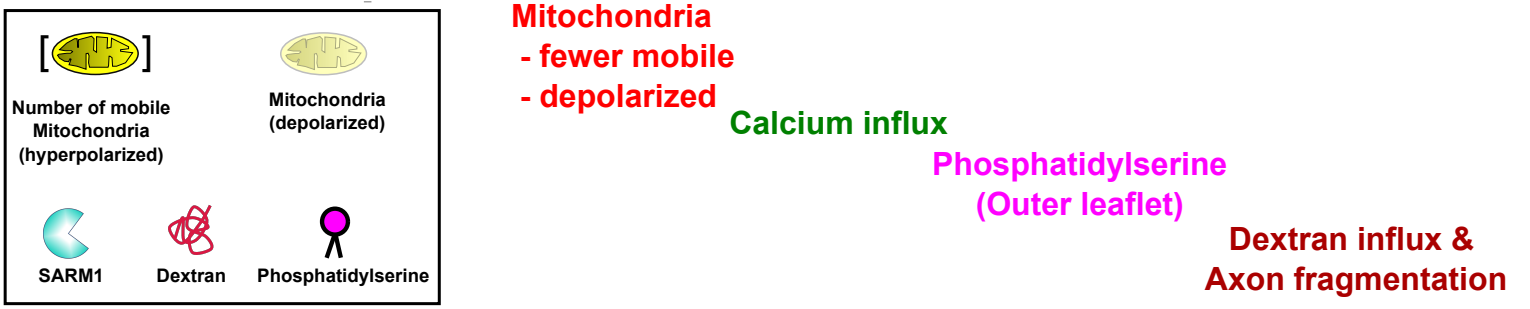

SARM1 activation

NAD^+ depletion

ATP loss

Mitochondria
- fewer mobile
- depolarized

Calcium influx

Phosphatidylserine
(Outer leaflet)

Dextran influx &
Axon fragmentation

Supple. 1

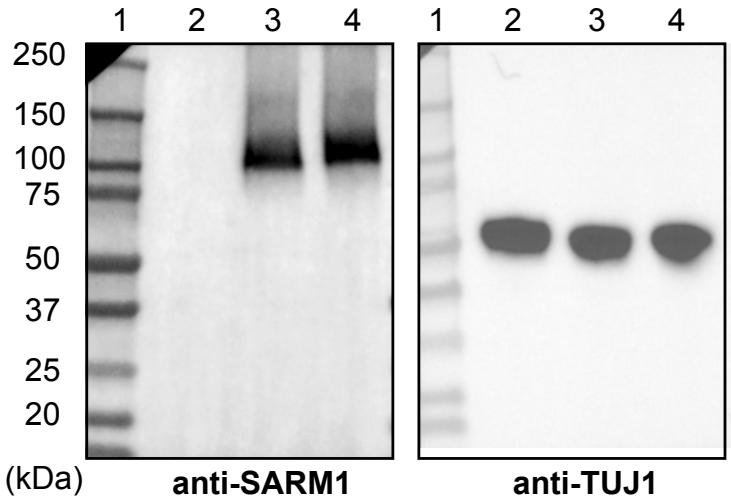

1. Marker
2. GFP
3. SARM1.WT
4. SARM1.E642A

Supple. 2

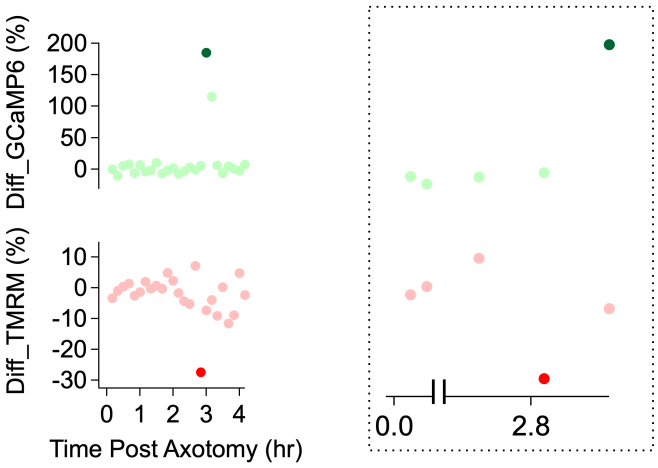

Supple 3

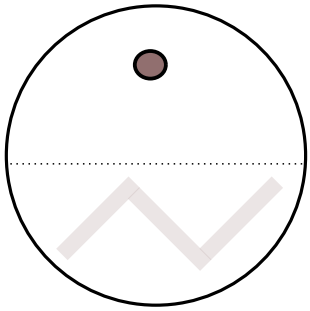

FluoroDish

2 µl suspension (~7 x 10^6 cells/ml)

2 µl suspension (~7 x 10^4 cells/ml)

Single axon imaging area

Supple. 4